



LAWRENCE
LIVERMORE
NATIONAL
LABORATORY

Implications of Pulser Voltage Ripple

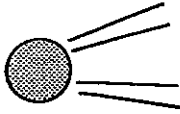
J. J. Barnard

December 22, 2011

Disclaimer

This document was prepared as an account of work sponsored by an agency of the United States government. Neither the United States government nor Lawrence Livermore National Security, LLC, nor any of their employees makes any warranty, expressed or implied, or assumes any legal liability or responsibility for the accuracy, completeness, or usefulness of any information, apparatus, product, or process disclosed, or represents that its use would not infringe privately owned rights. Reference herein to any specific commercial product, process, or service by trade name, trademark, manufacturer, or otherwise does not necessarily constitute or imply its endorsement, recommendation, or favoring by the United States government or Lawrence Livermore National Security, LLC. The views and opinions of authors expressed herein do not necessarily state or reflect those of the United States government or Lawrence Livermore National Security, LLC, and shall not be used for advertising or product endorsement purposes.

This work performed under the auspices of the U.S. Department of Energy by Lawrence Livermore National Laboratory under Contract DE-AC52-07NA27344.



To: HIF Note Mailing List
From: John Barnard
Subject: Implications of Pulser Voltage Ripple

In a recent set of measurements obtained by G. Kamin, W. Manning, A. Molvik, and J. Sullivan, the voltage waveform of the diode pulser had a ripple of approximately $\pm 1.3\%$ of the 65 kV flattop voltage, and the beam current had a larger corresponding ripple of approximately $\pm 8.4\%$ of the 1.5 mA average current at the location of the second Faraday cup, approximately 1.9 m downstream from the ion source. The period of the ripple was about 1 μs . It was initially unclear whether this large current ripple was in fact a true measurement of the current or a spurious measurement of noise produced by the pulser electronics. The purpose of this note is to provide simulations which closely match the experimental results and thereby corroborate the physical nature of those measurements, and to provide predictions of the amplitude of the current ripples as they propagate to the end of linear transport section. Additionally analytic estimates are obtained which lend some insight into the nature of the current fluctuations and to provide an estimate of what the maximum amplitude of the current fluctuations are expected to be, and conversely what initial ripple in the voltage source is allowed, given a smaller acceptable tolerance on the line charge density.

Simulations

1D HINJ simulations were carried out using the pulser voltage waveform that was obtained on 4 September 1996. The waveform was cutoff at 10 μs to afford a reasonable run time. HINJ is described in ref. 1. In these calculations, a greens function solution is used for particles within an ideal 1D (z) diode, but outside of the diode the fields are calculated using a particle-in-cell formalism, using the modified Poisson's equation described in ref. 1. On passage from the diode to the matching section the beam passes through a circular aperture reducing the current to 15 to 20% of the original current. This fraction is treated as a free parameter to match the dc component of the current pulse at a Faraday cup and for these runs is given by .177. In figure 1 we show, the beam current and energy at two Faraday cup locations ($z = 0.67$ m and $z = 1.89$ m), and the current and voltage supplied by the pulser at $z = 0$. Figure 2 shows an enlargement of the experimentally measured pulser voltage plot. Note that poor voltage resolution leads to some uncertainty in the exact amount of the energy ripple. Figure 3 shows a composite of both the HINJ simulation and experimental current measurement at the location of the second Faraday cup. In order to obtain good agreement of simulation with experiment, the time coordinate was shifted by 0.2 μs . This is believed to be due to a combination of a delay time between application of the voltage across the diode and measurement at the voltage monitor, and also a possible higher energy input to HINJ relative to the experiment. Given these caveats, the HINJ simulations show a relatively good agreement with the experiment suggesting that the current measurements are not the result of spurious noise signals. Finally, Figure

4 shows a HINJ prediction of the waveform at the end of the magnetic transport section, nearly 5 m from the source. The amplitude of the fluctuations is approximately $\pm 25\%$ of the average beam current, a value that is larger than is desired for insertion into the ring.

Estimate of Density Ripple Growth

The measurements indicate a quasi-sinusoidal voltage variation of amplitude 830 V about the nominal 65 kV flattop, corresponding to a fractional beam energy variation $\delta E/E_0 \cong \pm 0.013$. The corresponding longitudinal velocity perturbation is $\delta v/v_0 \cong \pm 0.0065$, where the nominal velocity of the potassium ion beam (mass 39) at 65 keV is 5.7×10^5 m/s.

We assume a voltage ripple applied to the diode at $z=0$ of the form

$$V(z = 0, t) = V_0 + \delta V \sin \omega t \quad (1)$$

giving rise to a ion velocity satisfying,

$$v(z = 0, t) \cong v_0 + \delta v \sin \omega t \quad (2)$$

Here $\delta V/V = 2\delta v/v$. Also, $\omega \cong 6.3 \times 10^6$ rad/s is the angular frequency of the 1 μ s voltage ripple. The spatial length between a peak and a trough in the velocity wave l_p (which is the half-wavelength of the perturbation), is initially given by $l_p = \pi v_0/\omega \cong 0.27$ m. One characteristic distance z_s is the propagation distance for the velocity shear in the sinusoidal perturbation to cause the peak to catch up with the trough. The distance z_s is the length over which wave steepening would become very apparent. If space charge forces can be neglected, z_s can be expressed as

$$z_s = \frac{v_0 l_p}{2\delta v} \cong 22 \text{ m} \quad (3)$$

Since the second Faraday cup is only located approximately 1.9 m downstream of the source, wave steepening should not be apparent. However, the change in l_p over 1.9 m is perceptible, giving rise to a perceptible density perturbation. The change in the half-wavelength δl_p is approximately $2(\delta v/v_0)z$, where z is the longitudinal distance from the source. Assuming the fractional change in the line charge density $\delta\lambda/\lambda_0$ is the same as the fractional change in l_p we find,

$$\frac{\delta\lambda}{\lambda_0} \cong \frac{\delta l_p}{l_p} \cong \frac{2\delta v}{\pi v_0} \left(\frac{\omega z}{v_0} \right) \quad (4)$$

At the second Faraday Cup at $z = 1.9$ m this corresponds to $\delta\lambda/\lambda_0 \cong 0.087$, roughly in agreement with the observed fractional current perturbation amplitude of 0.084. (In general, the fractional current perturbation $\delta I/I_0 = \delta\lambda/\lambda_0 + \delta v/v_0$. As will be shown $\delta v/v_0$ is usually much smaller than $\delta\lambda/\lambda_0$, so we have neglected the $\delta v/v_0$ term, in this comparison of the fractional line charge perturbation with the fractional current perturbation.)

Better Estimate of Ripple Growth

To obtain, a somewhat better estimate of the growth of current ripples, as well as estimate the requirement on the voltage pulser to deliver a specified current ripple tolerance, we may resort to the 1-D fluid equations (see, e.g. ref. 2). The continuity and momentum equations may be expressed as:

$$\frac{\partial \lambda}{\partial t} + \frac{\partial(\lambda v)}{\partial z} = 0 \quad (5)$$

$$\frac{\partial v}{\partial t} + v \frac{\partial v}{\partial z} = \frac{q}{m} E_z \quad (6)$$

Here q is the ion charge, m is the ion mass, and E_z is the longitudinal self electric field produced by fluctuations in the line charge density λ , assumed to be in the long wavelength limit (see, eg. ref.[3]),

$$E_z \cong -g \frac{\partial \lambda}{\partial z} \quad (7)$$

where $g = \ln(b/a)/2\pi\epsilon_0$ is the usual g -factor, b/a is the ratio of the pipe radius to average beam radius, and ϵ_0 is the free space permittivity. We may linearize equations (5) and (6) by letting $\lambda = \lambda_0 + \lambda_1$ and $v = v_0 + v_1$ where subscript 0 indicates equilibrium quantities and 1 indicates perturbed quantities. The linearized fluid and momentum equations are:

$$\frac{\partial \lambda_1}{\partial t} + v_0 \frac{\partial \lambda_1}{\partial z} + \lambda_0 \frac{\partial v_1}{\partial z} = 0 \quad (8)$$

$$\frac{\partial v_1}{\partial t} + v_0 \frac{\partial v_1}{\partial z} = \frac{-q}{m} g \frac{\partial \lambda_1}{\partial z} \quad (9)$$

Transforming to the comoving frame where $z' = z - v_0 t$ and $t' = t$, yields the simpler set:

$$\frac{\partial \lambda_1}{\partial t'} + \lambda_0 \frac{\partial v_1}{\partial z'} = 0 \quad (10)$$

$$\frac{\partial v_1}{\partial t'} + \frac{q}{m} g \frac{\partial \lambda_1}{\partial z'} = 0 \quad (11)$$

Taking the partial derivative of eq. (10) with respect to t and the partial derivative of eq. (11) with respect to z and combining yields (see e.g. ref. 5):

$$\frac{\partial^2 \lambda_1}{\partial t'^2} - \frac{q}{m} g \lambda_0 \frac{\partial^2 \lambda_1}{\partial z'^2} = 0 \quad (12)$$

We define a space charge wave speed $c_s \equiv (qg\lambda_0/m)^{1/2}$, and identify eq. (12) as the wave equation, with general solution (ref. [2], see also ref. [6]):

$$\lambda_1 = \lambda_0 [f_R(z' - c_s t') + f_L(z' + c_s t')] \quad (13)$$

$$v_1 = c_s [f_R(z' - c_s t') - f_L(z' + c_s t')] \quad (14)$$

Here $f_R(x)$ and $f_L(x)$ are arbitrary functions of the argument x , representing right and left traveling waves in the beam frame. Transforming back into the lab frame the solution becomes:

$$\lambda_1 = \lambda_0 [f_R(z - (v_0 + c_s)t) + f_L(z - (v_0 - c_s)t)] \quad (15)$$

$$v_1 = c_s [f_R(z - (v_0 + c_s)t) - f_L(z - (v_0 - c_s)t)] \quad (16)$$

To complete the solution we need to specify the boundary conditions at $z = 0$. Although we are primarily interested in the effects of small errors in voltage across a diode, it is also of interest to examine the effects of voltage errors across an induction gap, which have slightly different boundary conditions. Voltage perturbations across a diode give rise to current and velocity variations, whereas voltage perturbations across an induction gap give velocity variations but no current variation. Note that $z = 0$ corresponds to the location of the end of the diode, for diode voltage perturbations, and it corresponds to the center of an induction gap for induction gap voltage perturbations.

Boundary conditions for voltage variations across a diode. If the characteristic timescale of the perturbations is much longer than the transit time through the diode, then the steady-state Child-Langmuir law is valid for which the current $I \propto V^{3/2}$. Thus $I_1/I_0 = (3/2)V_1/V_0$. Also, since $qV = (1/2)mv^2$, $v_1/v_0 = (1/2)V_1/V_0$. Finally, since $I = \lambda v$, it follows that $\lambda_1/\lambda_0 = I_1/I_0 - v_1/v_0 = V_1/V_0$.

Boundary conditions for voltage variations across an induction gap. When the beam passes through an induction gap (of zero width) with a voltage perturbation, charge conservation requires that the instantaneous current be the same on both sides of the gap, so that $I_1/I_0 = 0$. However, as in the case of the diode perturbation, there is a velocity perturbation satisfying $v_1/v_0 = (1/2)V_1/V_0$, and therefore $\lambda_1/\lambda_0 = -(1/2)V_1/V_0$.

We let $V_1(z = 0, t)/V_0 \equiv g(t)$. At $z = 0$ the boundary conditions for both the diode and induction gap can be combined into a single pair of equations:

$$v_1 = \frac{v_0}{2} g(t) \quad (17)$$

$$\lambda_1 = \alpha \lambda_0 g(t) \quad (18)$$

where

$$\alpha \equiv \begin{cases} -\frac{1}{2} & \text{induction gap} \\ 1 & \text{diode} \end{cases} \quad (19)$$

Applying these boundary conditions to eqs. (15) and (16), allows us to solve for the general functions $f_R(x)$ and $f_L(x)$:

$$f_R(x) = \frac{1}{2} \left(\alpha + \frac{v_0}{2c_s} \right) g \left(\frac{-x}{(v_0 + c_s)} \right) \quad (20)$$

$$f_L(x) = \frac{1}{2} \left(\alpha - \frac{v_0}{2c_s} \right) g \left(\frac{-x}{(v_0 - c_s)} \right) \quad (21)$$

So the solution for all z, t which satisfy the boundary conditions at $z = 0$ is:

$$\frac{\lambda_1}{\lambda_0} = \frac{1}{2} \left(\alpha + \frac{v_0}{2c_s} \right) g \left(t - \frac{z}{(v_0 + c_s)} \right) + \frac{1}{2} \left(\alpha - \frac{v_0}{2c_s} \right) g \left(t - \frac{z}{(v_0 - c_s)} \right) \quad (22)$$

$$\frac{v_1}{c_s} = \frac{1}{2} \left(\alpha + \frac{v_0}{2c_s} \right) g \left(t - \frac{z}{(v_0 + c_s)} \right) - \frac{1}{2} \left(\alpha - \frac{v_0}{2c_s} \right) g \left(t - \frac{z}{(v_0 - c_s)} \right) \quad (23)$$

Also, we may calculate I_1/I_0 :

$$\begin{aligned} \frac{I_1}{I_0} = & \frac{1}{2} \left(\alpha + \frac{1}{2} + \frac{\alpha c_s}{v_0} + \frac{v_0}{2c_s} \right) g \left(t - \frac{z}{(v_0 + c_s)} \right) \\ & + \frac{1}{2} \left(\alpha + \frac{1}{2} - \frac{\alpha c_s}{v_0} - \frac{v_0}{2c_s} \right) g \left(t - \frac{z}{(v_0 - c_s)} \right) \end{aligned} \quad (24)$$

(When $\alpha = -1/2$, we recover the same leading coefficient in eq. (2) of ref. 6). We now let $V_1/V_0(z=0, t) \equiv g(t) = 2(\delta v/v_0) \sin \omega t$. Using the approximation that $1/(v_0 \pm c_s) \cong (1/v_0)(1 \mp c_s/v_0)$, equations (22) through (24) yield:

$$\frac{\lambda_1}{\lambda_0} \cong \frac{\delta v}{c_s} \left(\cos[\omega(t - \frac{z}{v_0})] \sin \frac{\omega c_s}{v_0^2} z + 2\alpha \frac{c_s}{v_0} \sin[\omega(t - \frac{z}{v_0})] \cos \frac{\omega c_s}{v_0^2} z \right) \quad (25)$$

$$\frac{v_1}{c_s} \cong \frac{\delta v}{c_s} \left(\sin[\omega(t - \frac{z}{v_0})] \cos \frac{\omega c_s}{v_0^2} z + 2\alpha \frac{c_s}{v_0} \cos[\omega(t - \frac{z}{v_0})] \sin \frac{\omega c_s}{v_0^2} z \right) \quad (26)$$

$$\begin{aligned} \frac{I_1}{I_0} \cong & \frac{\delta v}{c_s} \left(\left[1 + 2\alpha \left(\frac{c_s}{v_0} \right)^2 \right] \cos[\omega(t - \frac{z}{v_0})] \sin \frac{\omega c_s}{v_0^2} z \right. \\ & \left. + (2\alpha + 1) \frac{c_s}{v_0} \sin[\omega(t - \frac{z}{v_0})] \cos \frac{\omega c_s}{v_0^2} z \right) \end{aligned} \quad (27)$$

Note that in equations (25) through (27) the first term in each equation is the dominant one and is of order $\delta v/c_s$. Thus current perturbations eventually grow to the level of $\delta v/c_s$, which is usually much larger than the initial fractional voltage perturbation $\delta V/V_0 = 2\delta v/v_0$ since usually $c_s \ll v_0$.

Now we may calculate some of the quantities of interest using the parameters of the recirculator beam. For $b/a \cong 1.9$, the space charge g-factor is $g = 1.16 \times 10^{10}$ V/C. The line charge density $\lambda_0 \cong 2.6 \times 10^{-9}$ C/m for the 65 keV, 1.5 mA potassium beam. The space charge wave velocity can be expressed in terms of the perveance $K = q\lambda_0/(2\pi\epsilon_0 m v_0^2)$:

$$c_s = \left(\frac{q}{m} g \lambda_0 \right)^{1/2} = v_0 \left(K \ln \frac{b}{a} \right)^{1/2} \quad (28)$$

For the parameters above, $c_s \cong 8.7 \times 10^3$ m/s. This compares with a perturbation velocity $\delta v = 3.5 \times 10^3$ m/s, which yields the ratio:

$$\frac{\delta v}{c_s} \cong 0.42 \quad (29)$$

As noted earlier, the maximum amplitude of the line charge density is given roughly by eq. (29). This maximum amplitude in the line density is reached when the argument of the sine in the first term of eq. (25) approximately equals $\pi/2$, i.e. when $z \cong z_{\lambda_{max}}$ where

$$z_{\lambda_{max}} = \frac{\pi v_0^2}{2\omega c_s} \quad (30)$$

For the parameters above $z_{\lambda_{max}} \cong 9.3$ m. (If voltage corrections are made to the pulse at a point down the beamline, it was found in ref. [6] that $z_{\lambda_{max}}$ is the maximum distance allowed before space charge effects make it practically difficult to remove such voltage errors.)

Having such large density perturbations as implied by eq. (29), could have serious consequences in the beam transport through the recirculator. If we allow maximum density perturbations $(\delta\lambda/\lambda_0)_{max}$ of, say, a few per cent then a relevant question is "what is the maximum allowed energy ripple $(\delta E/E_0)_{max}$?" Since

$$\left(\frac{\delta E}{E_0}\right)_{max} = 2 \left(\frac{\delta v}{v_0}\right)_{max} = 2 \frac{c_s}{v_0} \left(\frac{\delta v}{c_s}\right)_{max} = 2 (K \ln(b/a))^{1/2} \left(\frac{\delta\lambda}{\lambda_0}\right)_{max}, \quad (31)$$

we find that the required $(\delta E/E_0)_{max}$ for our parameters is about 0.03 $(\delta\lambda/\lambda_0)_{max}$, or about 1.5×10^{-3} for a 5% allowed line charge perturbation. This is a somewhat more stringent energy variation requirement than had been given in our original injector specifications given to Titan Beta (ref[4]). (We originally had specified $\pm 0.5\%$ energy variation.) Note also that since the small recirculator perveance is only a factor of ~ 3 smaller than the LBNL ESQ injector perveance, with similar values of $\ln b/a$, we find that the allowed energy ripple is smaller by a factor of 1.7 than the allowed ripple for the LBNL ESQ injector, assuming the same allowed current variation. For completeness we note (see e.g. refs [7] and [8]) that pulse compression sets an independent requirement on the energy flatness, to insure acceptable chromaticity through the final optic.

Comparison of Experiment, Simulation, and Theory

Table 1 shows a comparison of measured and calculated values of current and energy perturbations at the indicated z locations. For the experiment and simulation, we have estimated half the peak to trough difference for the second apparent sinusoidal ripple in the data. The theory is obtained using eqs. (25) through (27), $\alpha = 1$, and using $\delta E/E = 2\delta v/v_0$. Although in qualitative agreement, the theory and simulation predict a larger current perturbation than is experimentally observed. This may be due to the poor resolution of the digitized voltage waveform which is used as input to both HINJ

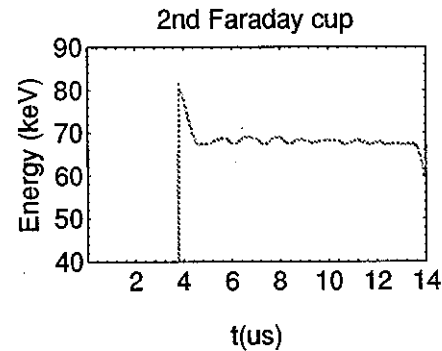
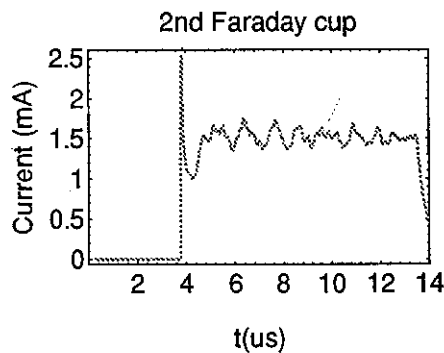
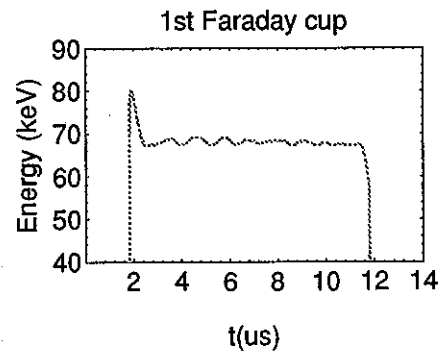
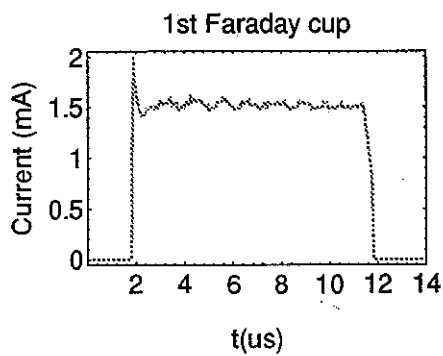
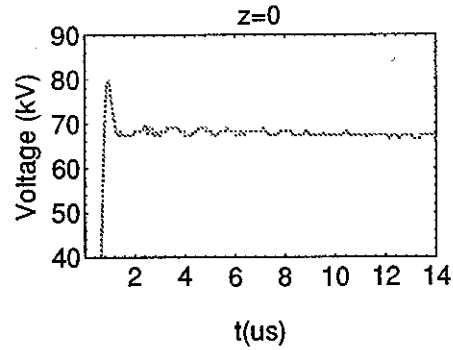
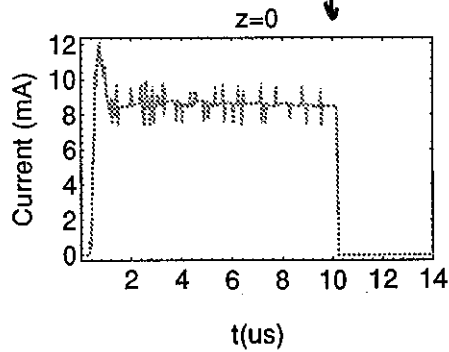
and theory. The initial conditions could have nearly 50% smaller amplitude and still be consistent with the digitization of the waveform.

Acknowledgments

The author would like to thank Steve Lund for critically reading a prior version of this note and his useful suggestions, Tom Fessenden for pointing out the correct boundary condition at an induction gap and other useful insights, and George Kamin, Art Molvik, and Bill Manning for providing the experimental waveforms and additional helpful discussions.

References

- [1.] 1993, J. J. Barnard, G. Caporaso, and S. S. Yu, "1-D Simulations of Heavy Ion Injectors," Proceedings of the 1993 Particle Accelerator Conference, Washington, D.C., May, 1993. 1, 712.
- [2.] See, for example, L.D. Landau, and E.M. Lifshitz, "Fluid Mechanics," 1959, [Pergamon Press, Oxford].
- [3.] M. Reiser, "Theory and Design of Charged Particle Beams," [Wiley & Sons, New York], 1994.
- [4.] John Barnard and Tom Fessenden, Memo to Shmuel Eylon and Ken Whittum, Subject: Injector Specification, December 17, 1993.
- [5.] A.I. Warwick, T.J. Fessenden, D. Keefe, C.H. Kim, H. Meuth, "Performance of MBE-4, an Experimental Multiple Beam Induction Accelerator for Heavy Ions," Proceedings of the European Particle Accelerator Conference, p. 118, June, 1988.
- [6.] Fessenden, Thomas J., "Emittance Variations in Current-Amplifying Ion Induction Linacs," 1991 IEEE Particle Accelerator Conference, p. 586 [IEEE, San Francisco].
- [7.] A. Warwick and E.P. Lee, "Accelerator errors in MBE-4 and in a driver," HIFAR note 214, (1988).
- [8.] Lee C. Teng, "Accelerator Parameters," ERDA Summer Study of Heavy Ions for Inertial Fusion, Claremont Hotel, Oakland/Berkeley, California July 19-30, 1976, Final Report, p. 13 (1976).

FIGURE 1(CURRENT TERMINATED AT $10 \mu s$)

NOTES:

1. CURRENT TRANSMISSION THROUGH DIODE PLATE ASSUMED TO BE 0.1771 TO MATCH D.C. CURRENT LEVEL
2. TIMESHIFT OF CURRENT WAVEFORMS W.R.T. VOLTAGE PULSE OF $0.20 \mu s$, PERHAPS DUE TO DELAY TIME OF VOLTAGE MONITOR.

FIGURE 2

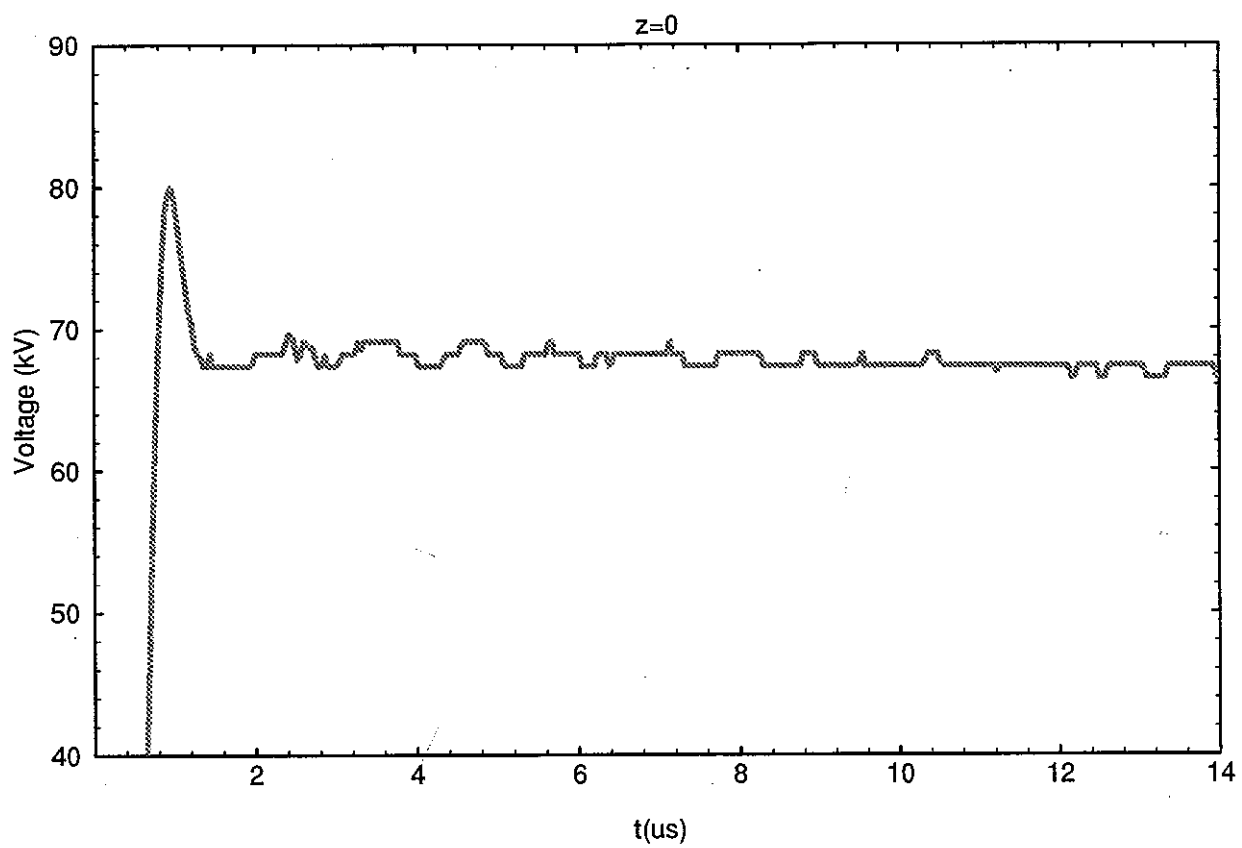


FIGURE 3

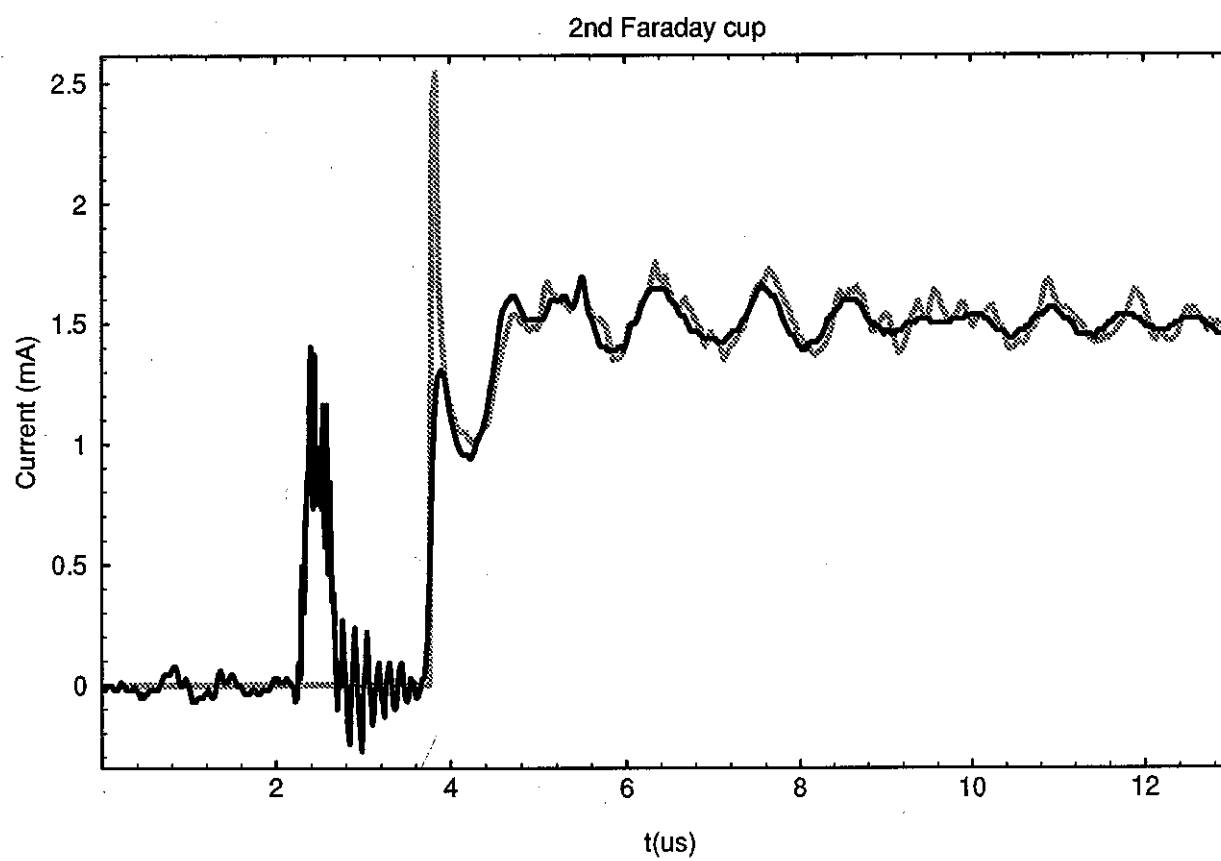
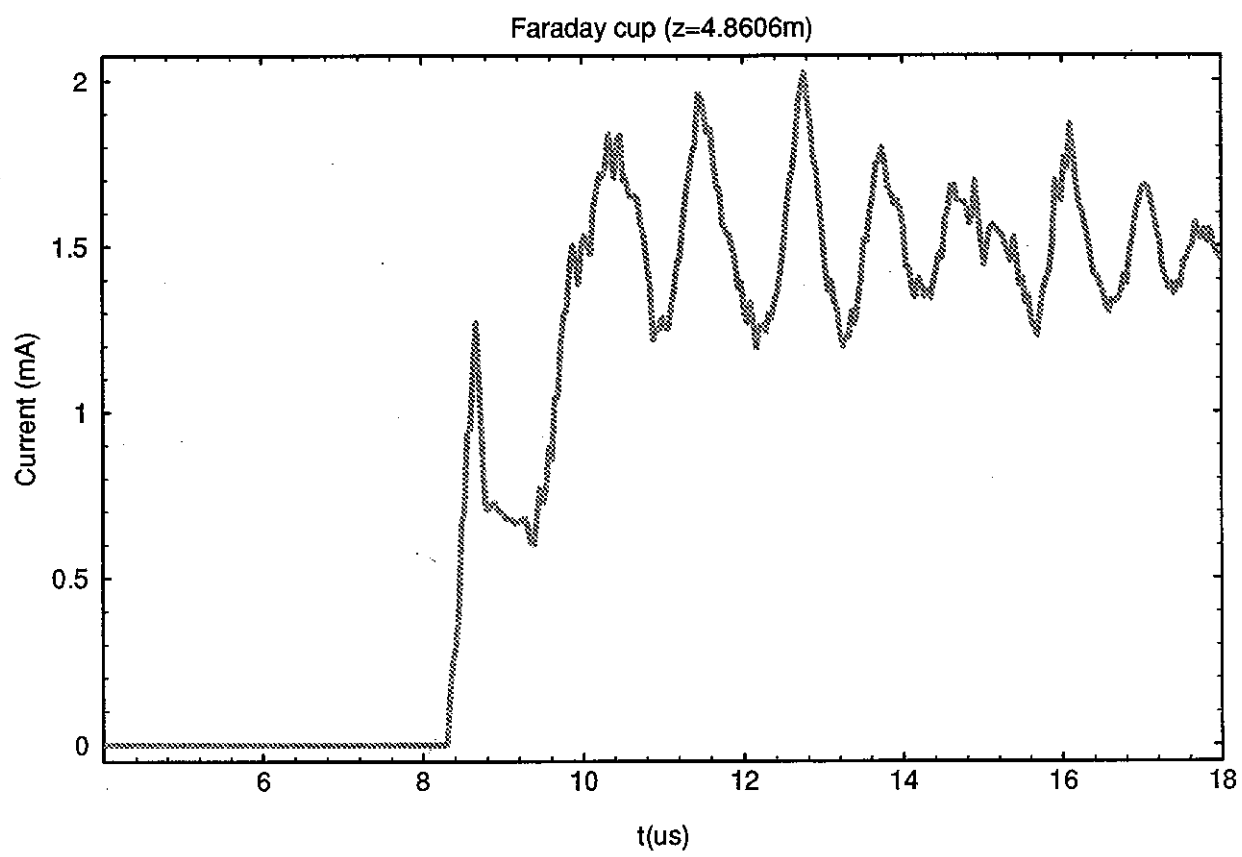


FIGURE 4



Comparison of Experiment, Simulation and Theory

	<u>Experiment</u>		<u>HINJ</u>		<u>Theory</u>	
	$\Delta I/I_0$	$\Delta E/E_0$	$\Delta I/I_0$	$\Delta E/E_0$	$\Delta I/I_0$	$\Delta E/E_0$
z=0		0.013	~.02	0.013	0.0195	0.013
First Faraday cup z=0.67m			0.067	0.013	0.067	0.013
2nd Faraday Cup z=1.89 m	0.084		0.133	0.013	0.151	0.012
End of Magnetic Transport Section z=4.86 m			0.250	0.0065	0.321	0.0091

Table 1.